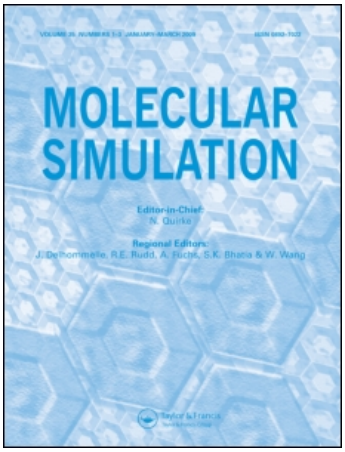

Molecular Simulation
Publication details, including instructions for authors and subscription information:
http://www.informaworld.com/smpp/title~content=t713644482

Application of Computer Simulation Methods to the Study of Metal Sulphide Minerals

K. Wright[a]; D. J. Vaughan[a]
[a] Dept. of Earth Sciences, University of Manchester, Manchester, UK

To cite this Article Wright, K. and Vaughan, D. J.(1998) 'Application of Computer Simulation Methods to the Study of Metal Sulphide Minerals', Molecular Simulation, 21: 2, 89 — 103
To link to this Article: DOI: 10.1080/08927029808022053
URL: http://dx.doi.org/10.1080/08927029808022053

Molecular Simulation, 1998, Vol. 21, pp. 89–103
Reprints available directly from the publisher
Photocopying permitted by license only

APPLICATION OF COMPUTER SIMULATION METHODS TO THE STUDY OF METAL SULPHIDE MINERALS

K. WRIGHT* and D. J. VAUGHAN

Dept. of Earth Sciences, University of Manchester, Oxford Road, Manchester M13 9 PL UK

(Received September 1997; accepted January 1998)

The crystal chemistry of metal sulphide minerals is an important area of study with applications to the environment and to the extraction of metal ores. In this paper, we present an overview of computational modelling studies as applied to the bulk and surface properties of metal sulphides. The emphasis is on applications rather than techniques and in order to illustrate work in this field, we focus on the ZnS polymorphs, pyrite (FeS_2) and phases with the galena (PbS) structure.

Keywords: Computer simulation; metal sulphides; pyrite; galena; sphalerite

INTRODUCTION

The metal sulphides are an important group of minerals exhibiting a variety of structure types and properties. Although most of the structures have been well characterised, the details of site occupancies and valence states in some phases is still uncertain. Deviations from stoichiometric compositions are a feature of many sulphide minerals. In phases such as ZnS and PbS, deviations from the ideal stoichiometry are small but can significantly influence electrical properties. In other minerals, the deviations may be more extreme, as exhibited by the pyrrhotites ($Fe_{1-x}S$), where variations in the ordering schemes of Fe vacancies that take place on cooling lead to a range of structures. Each has a small difference in stability, so that phase relations are complex at low temperatures.

*Corresponding author.

The great diversity of electrical and magnetic properties displayed by metal sulphides make them important technological materials. For example, Fe sulphides have been investigated as possible materials for solar cells and solid state batteries, whereas ZnS is an important semiconductor used in certain optoelectrical devices. Sulphide minerals are the major source of many of the worlds production of base metals (Cu, Pb, Zn), certain ferroalloy metals (Mo, Co, Ni) and many rare and precious metals (Ga, Ge, In, Pt, Os *etc.*).

Nearly all sulphide minerals are highly reactive in oxidising environments and are a potential source of pollution. At former mining sites, the waste material from mineral extraction and processing is often exposed to weathering reactions. Fe sulphides can react with oxygen rich-waters to produce very acid solutions (acid mine drainage) and these solutions can cause further damage by breaking down minerals containing toxic elements (*e.g.*, Pb, As, Hg, Cd) and releasing them into the environment.

In this paper, we look at some of the ways in which computational modelling techniques can be used to investigate the bulk and surface properties of selected sulphides. Bulk studies are used to understand and predict equilibrium crystal structures and unit cell parameters and their variation with pressure and temperature, to predict a range of physical properties of the ideal crystal, and to investigate the nature of defects and their influence on bulk properties. Computational modelling of surfaces is primarily concerned with predicting geometric structures, their reactivities and the products of reactions at surfaces, particularly oxidation.

In order to illustrate work in this large and growing field, we will focus discussion on three important and contrasting families of metal sulphide minerals: (i) those related to the ZnS polymorphs, sphalerite and wurtzite; (ii) those related to the mineral pyrite (FeS_2), and (iii) those related to galena (PbS). Emphasis will be on our own studies involving both atomistic and electronic structure methods. The background to the application of such methods to mineral systems is discussed in much greater detail elsewhere [1, 2].

ZnS AND RELATED MINERALS

Sphalerite and wurtzite, respectively the cubic and hexagonal polymorphs of ZnS, both have structures in which Zn is in tetrahedral coordination to S and all tetrahedra share corners. The electronic structure of ZnS has been of considerable interest because of the importance of this material as a semiconductor and, hence, the subject of numerous calculations. For

example, Bernard and Zunger [3] used a density functional approach in a detailed calculation which yielded the band structure shown in Figure 1(a) and the charge density contours for the valence band (Fig. 1(b)). These and similar calculations [4–7] provide information on the stable crystal structures and on electronic properties such as the band gap.

In other studies, calculations on just the ZnS_4^{6-} tetrahedral cluster provide information on the local electronic structure and on phenomena which are localised in character. For example, calculations using the MS-SCF-Xα method [8, 9] facilitated interpretations of optical and X-ray spectra. In Figure 2, results of such a calculation on the ZnS_4^{6-} cluster show molecular orbital energy levels labelled according to the irreducible representations of the T_d symmetry group. Results are given here for both the ground state (GS) configurations and using the transition state (TS) procedure which incorporates electronic relaxation effects occurring during ionisation. As can

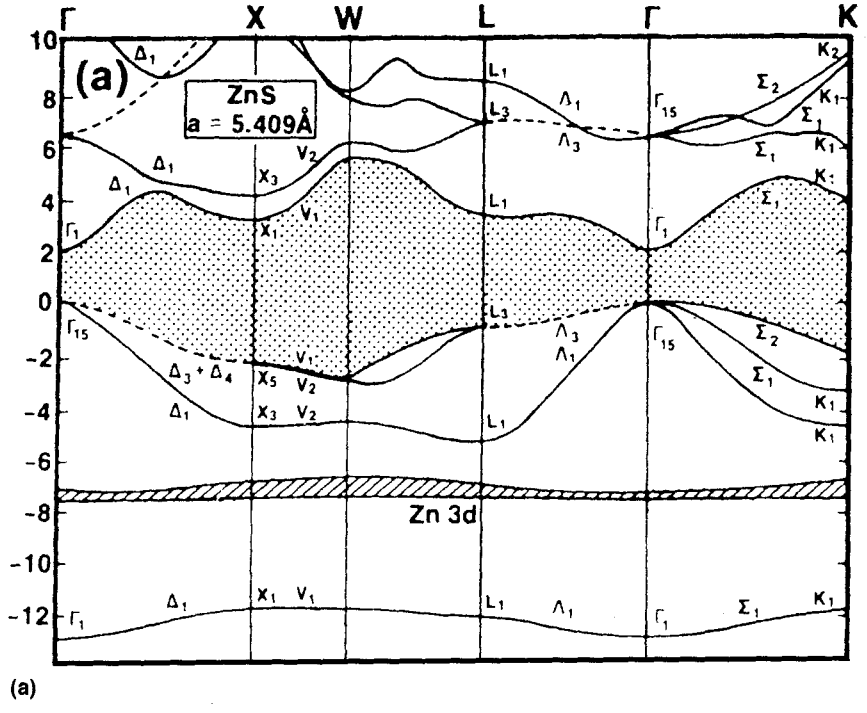

(a)

FIGURE 1 The electronic structure of sphalerite (ZnS) from a self consistent local density band structure calculation: (a) band structure showing the fundamental band gap region (shaded) and the Zn 3*d* levels (hatched); (b) plot of the charge density contours for the valence band of ZnS (logarithmically spaced in units of e/a.u^3). Solid circles represent core regions. (After [3]; reproduced with publishers permission).

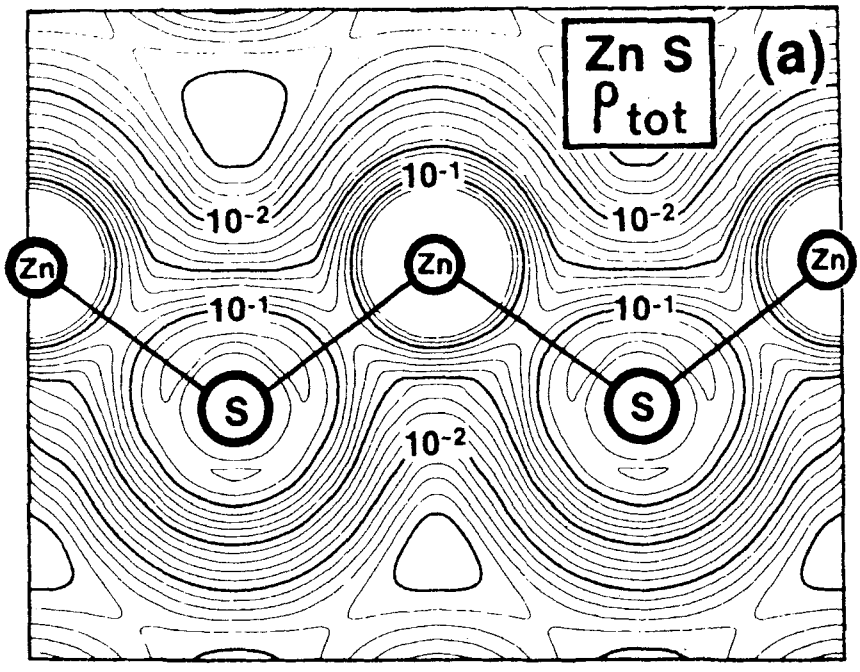

FIGURE 1 (Continued).

be seen from Figure 2, the latter show quite good agreement with peaks in the X-ray emission (XES) and X-ray photoelectron (XPS) spectra.

Other calculations are based on atomistic models which have been used to predict the structure of the perfect lattice and the nature of defects [10]. In any atomistic simulation, the quality of the results will depend on the ability of the potential parameters used to accurately describe atomic interactions in the solid. The parameters used in the study were developed by empirical fitting to experimental data [10] and accurately reproduce the measured structure and properties of sphalerite as shown in Table I. The calculated properties are also in reasonable agreement with those of wurtzite.

Atomistic calculations have been particularly successful in predicting the behaviour of defects and have been shown to accurately predict defect formation energies and geometries [11]. Wright and Jackson [10] have calculated defect formation and migration energies for Zn and S in both polytypes of ZnS. The results indicate that formation of Schottky and Frenkel defects is more favoured when they are bound than when they are assumed to be non-interacting. The most favourable defect in wurtzite, *i.e.*, that with the lowest formation energy (Tab. II), is the ZnS Schottky pair,

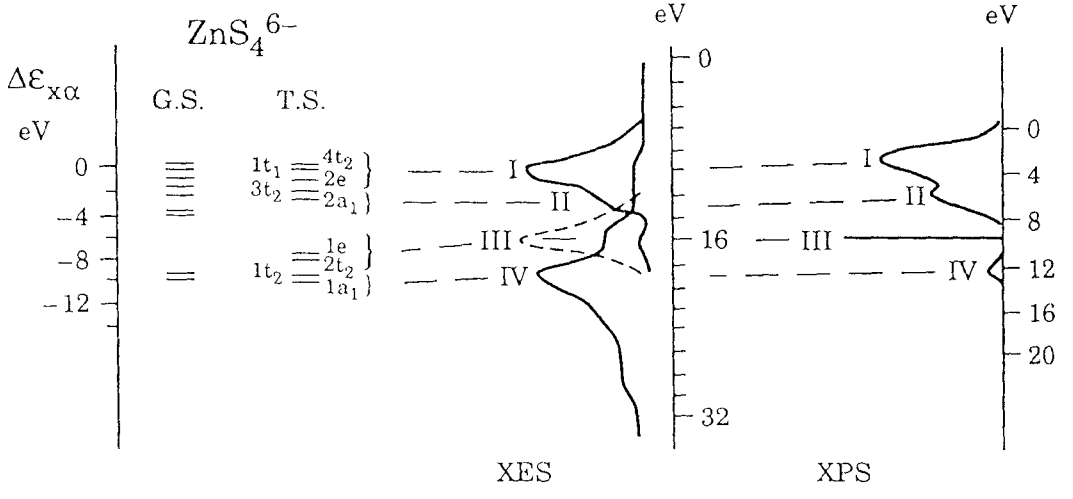

FIGURE 2 Valence region XES and XPS spectra for ZnS compared to MS-SCF-Xα cluster calculation results, both for the ground state (G.S.) and transition state (T.S.). (After [1]; reproduced with publishers permission).

whereas for sphalerite, the Zn Frankel defect has a slightly lower energy than the Schottky defect.

The defect calculations were extended to the prediction of atomic migration activation energies, which are summarised in Table III. Calculated values of migration activation energy are in reasonable agreement with experimental data and on the basis of these Arrhenius energies, a model for diffusion in ZnS was put forward, whereby Zn migrates *via* an interstitial or interstitialcy mechanism, but S does so by way of vacancies.

TABLE I Comparison of experimental and calculated structural and elastic data for the sphalerite and wurtzite forms of ZnS

	Sphalerite		*Wurtzite*	
Parameter	*Expt.*	*Calc.*	*Expt.*	*Calc.*
Unit cell dimenstion (Å)				
a	5.41	5.407	3.85	3.91
b			3.85	3.91
c			6.29	6.05
Axial ratio a/c			6.12	6.46
Cell volume (Å^3)	158.297	158.10	84.75	80.18
Elastic constants (GPa)				
C_{11}	94.2	91.7	121.2	108.5
C_{12}	56.8	58.2	66.3	54.9
C_{13}			50.9	53.2
C_{33}			140.8	86.8
C_{44}	43.6	44.0	28.6	26.8
C_{66}			32.4	34.4
Dielectric constants				
εstat	7.9	7.33	4.086	
εhf	5.6–6.1	5.98		

TABLE II Calculated defect formation energies (δE_f) for bound defects and binding energies (E_B) in sphalerite and wurtzite. Values in brackets are formation energies per defect

	Sphalerite		*Wurtzite*	
Defect	E_B	$\Delta E_f(eV)$	*E B*	$\Delta Ef(eV)$
ZnS Schottky	−2.47	3.53 (1.77)	−2.3	4.4 (2.20)
Zn Frenkel	−3.62	3.32 (1.66)	−2.0	5.8 (2.90)
S Frenkel	−0.7	6.8 (3.40)	−2.1	6.4 (3.2)

TABLE III Calculated Arhenius energies (ΔE) in eV for sphalerite and wurtzite

Species	*Mechanism*	ΔE *sphalerite*	ΔE *wurtzite*
Zn	Vacancy	1.15	1.23
Zn	Interstitial	0.8	0.85
S	Vacancy	1.4	1.58
S	Interstitial	1.9	2.10

There have been a number experimental studies on the surface structure of ZnS and related materials. Studies using XPS, low energy electron diffraction (LEED) and theoretical methods have shown that the ZnS {110} surface undergoes considerable relaxation from the bulk termination [12]. This phenomenon is also observed in other semiconductor compounds with the sphalerite structure (*e.g.*, GaAs, ZnSe, CdTe). The calculations of Wright *et al.* [13] suggest a similar relaxation on the {110} surfaces (Fig. 3) with both horizontal and vertical displacements of atoms in the surface layer. However, the vertical displacements predicted by this model are somewhat less than those inferred from experimental data.

Sphalerite normally exhibits small deviations from stoichiometry [14] and excess S or Zn at the surface could lead to changes in the surface energy. Wright *et al.* [13] have computed the energy of the {100}, {110} and {111} surfaces containing point defects. Surface non-stoichiometry was simulated by the introduction of point defects into the surface layer as illustrated in Figure 4. The results predict that for Zn-poor compositions the (111) surfaces will be more stable than the {110} while for Zn-rich compositions are $(\bar{1}\bar{1}\bar{1})$ face is stabilised relative to {110}. These calculations show that variations in stoichiometry leading to a change in valence states of

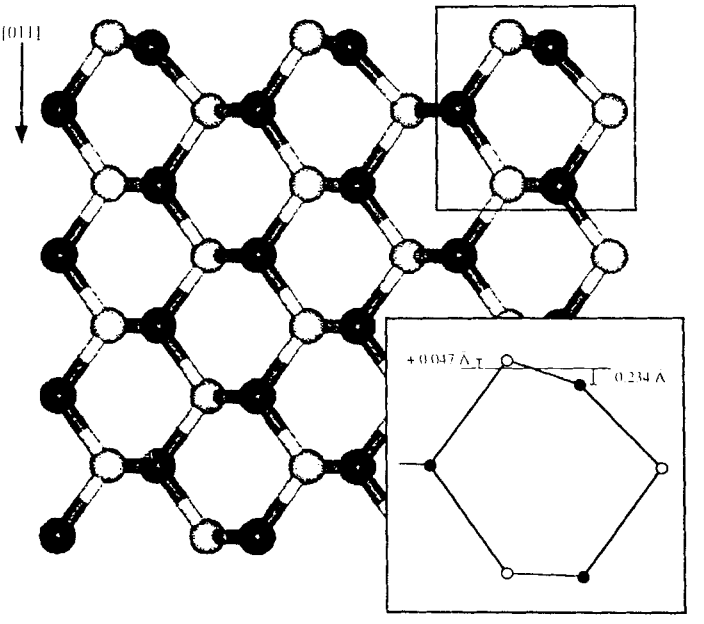

FIGURE 3 Relaxation of the surface atoms for the (110) surface of sphalerite (ZnS) as calculated by [13]. Inset sketch shows the amount of movement in the vertical plane.

(111)S	D	$(\bar{1}\bar{1}\bar{1})$Zn
-S---S---S--S_i	0.00	Zn--V_{Zn}--Zn--
-Zn^+--Zn--Zn^+--Zn	0.14	-S^----S---S---S^---
-S---S---S---S--	0.57	-Zn--Zn--Zn--Zn
-Zn--Zn--Zn--Zn	0.72	-S---S---S---S--
--S--	1.15	-Zn--

FIGURE 4 A sulphur rich surface on sphalerite (ZnS) created by introducing S interstitials or Zn vacancies. Charge balance is maintained by changing the valence state of adjacent Zn or S atoms. (After [13]).

surface species can have a pronounced effect on surface energies. However, the change in valence states of S and Zn associated with surface non-stoichiometry could equally well be achieved by the addition of impurities such as Cl^-, Ni^{3+} and Cd^{3+}.

FeS_2 AND RELATED MINERALS

Pyrite, (FeS_2), the most abundant natural sulphide has a crystal structure in which iron is octahedrally coordinated to S_2^{2-} dianion units. It is a diamagnetic semiconductor with an experimentally determined band gap of ~ 0.9 eV. Hence the octahedrally coordinated Fe^{2+} in pyrite is in a low-spin state with an electronic configuration of $(t_{2g})^6$ $(e_g)^0$. As in the case of ZnS, a substantial number of computational studies have been undertaken on FeS_2 as well as on several isostructural phases (*e.g.*, CoS_2, NiS_2, CuS_2, ZnS_2). For example, Temmerman *et al.* [15] used a local density approximation band structure method to calculate the electronic structures of pyrite-type disulphides. For FeS_2, the calculation gave an equilibrium cell volume within 3.3% of that determined experimentally and a reasonable value for the band gap of 0.64 eV. As illustrated in Figure 5, this calculation provided information on the density of states for 10 eV above and below the Fermi Level. As well as the total density of states, the calculations also show the extent to which iron and sulphur each contribute to the filled energy states of the valence band and empty states of the conduction band. These local densities of states have been used in turn to calculate XPS spectra and Bremsstrahlung Isochromat spectra which show good agreement with experiment [15]. Other theoretical studies of pyrite undertaken using

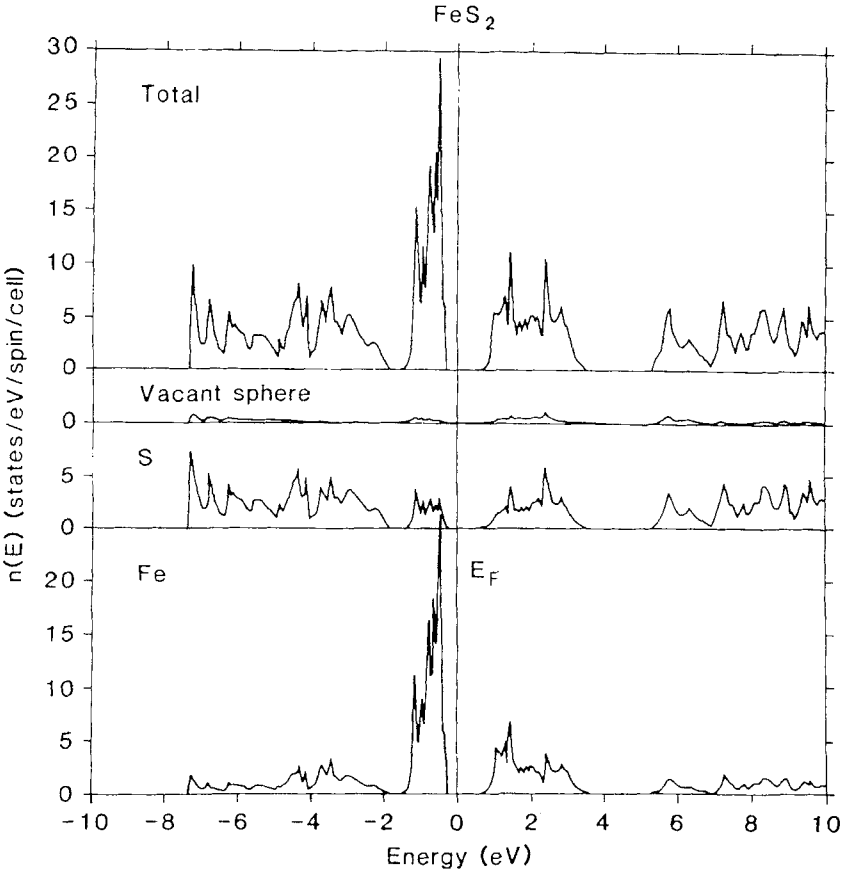

FIGURE 5 Density of states calculated for 10 eV above and below the Fermi level for pyrite (FeS_2). Total density of states is shown at the top of the figure and below this the contribution from sulphur states and iron states; and "vacant sphere" states added to improve the calculation. (After [15]; reproduced with publishers permission).

quantum mechanical methods [16–18] have achieved varying levels of agreement with measured properties (*e.g.*, band gap values calculated as from 0.74 to 0.52 eV). Cluster calculations on the FeS_6^{10-} unit [8, 19] again provide insight into local electronic structures around iron and the other metals in the pyrite structure (Co, Ni, Cu, Zn) and the interpretation of properties influenced by local structure.

More recently, atomistic methods have been used to model the bulk properties of pyrite. Potential parameters for FeS_2 have been developed [20] using the same methodology as for ZnS [10]. A comparison of calculated and experimental structural parameters for pyrite and its metastable

polymorph marcasite are given in Table IV. The agreement is extremely good for pyrite, with all values to within less than 1% of those determined by experiment. However, in the case of marcasite (Tab. V), the fit is not so good with the c/a ratio being too large.

The elastic behaviour of pyrite has been well studied because of early reports of a negative value for C_{12}. More recent experiments [21] have shown C_{12} to be positive. The atomistic model [20] gives a value for the bulk modulus of 157 GPa, within 0.5% of the experimental values (155 GPa) reported by Battenbatouche *et al.* [21]. These authors also carried out experiments at pressures up to 0.2 GPa. Their results are compared with calculated values in Table VI where it can be seen that although the agreement is reasonable, the shear component of the compressibility is somewhat underestimated by the model at high pressure.

TABLE IV Comparison of experimental and calculated properties of pyrite. (Elasticity data from [21])

Property	*Experiment*	*Calculated*
a (Å)	5.418	5.408
vol. (Å^3)	159.04	158.185
S–S(Å)	2.177	2.171
Fe–S (Å)	2.262	2.258
C_{11}(GPa)	366.0 (±0.2)	373.0
C_{12}	49.0 (±1.0)	48.6
C_{33}	103.0 (±1.0)	103.9
Phonon range cm^{-1}	211–440	187–440

TABLE V Comparison of experimental and calculated properties for marcasite

Property	*Experiment*	*Calculated*
a (Å)	4.436	4.11
b (Å)	5.414	5.43
c (Å)	3.381	3.62
c/a	0.88	0.76
c/b	0.67	0.62
vol. (Å^3)	81.20	80.897
S–S(Å)	2.21	2.206
Fe–S (Å)	2.23	2.265
	2.25	2.259

TABLE VI Experimental and calculated pressure derivatives of the elastic moduli of pyrite at 0.2 GPa. Experimental data from [21]

Pressure derivatives	*Experimental*	*Calculated*
$\partial C_{11}/\partial P$	13.3(±1.0)	12.2
$\partial C_{12}/\partial P$	4.1(±2.0)	1.6
$\partial C_{44}/\partial P$	1.7(±1.0)	2.7

PbS AND RELATED MINERALS

Galena (PbS), along with PbSe, PbTe (clausthalite and altaite) and the phases CaS (oldhamite) and MgS (niningerite) which occur only in meteorites, has the simple cubic NaCl structure, with all atoms in regular octahedral coordination. The electronic structure of PbS has been studied in considerable detail because of its semiconducting properties (band gap ~ 0.4 eV). Band structure calculations and molecular orbital (MO) calculations on large clusters such as SPb_6 $S_{12}Pb_8$ [22] have also been used to investigate the electronic structure of PbS. In addition, *ab initio* Hartree–Fock methods have been applied to the study of the bulk properties in galena [23], where the calculated lattice parameter and elastic constants were in reasonable agreement with experimental values.

As well as the above, there have been a number of computational studies on the isostructural phases CaS and MgS. These have concentrated primarily on the bulk moduli and pressure induced structural phase transformations. The results are summarised in Table VII. Experiments carried out on MgS to 54 GPa [24] show no change in structure. However, semi-empirical tight binding calculations [25] predict a transition from the NaCl (B1) structure to the CsCl (B2) at 64 GPa, whilst our own preliminary atomistic calculations (unpublished) give a transition pressure of approximately 58 GPa, both of which are consistent with the experimental findings. The calculation of bulk modulus however, is underestimated by the semi-empirical method (56 GPa) [25] and overestimated by atomistic techniques (96 GPa) when compared to the experimental value [24] of 78.9 GPa. In the case of CaS, the atomistic and semi-empirical results both suggest a B1 to B2 transition at around 35 GPa

Experimental evidence from low energy electron diffraction (LEED) and scanning tunnelling microscopy (STM) studies [26, 27] indicate that the {001} surface of galena, unlike the (110) ZnS surface, exhibits only minimal

TABLE VII Summary of experimental and computational data for the zero pressure bulk modulus (B_0) and B1→B2 transition pressure of CaS and MgS. The different computational techniques are electron-gas (EG), atomistic (A) and tight binding (TB)

	Exp.	*Calc. (EG)*	*Calc. (A)*	*Calc. (TB)*
CaS				
B_0(GPa)	52.4	62.3	81.0	42.0
$P_{trans.}$(GPa)	40.0	42.0	37.5	35.5
MgS				
B_0(GPa)	81.4	84.1	96.0	59.0
$P_{trans.}$(GPa)	None up to 54 GPa	105.0	58.0	64.0

relaxation from the bulk truncated solid. There are, nevertheless, likely to be various defects at the surface, associated with steps and with S and Pb vacancies (see Fig. 6). Although the experimental data show no significant movement (relaxation) of atoms at the surface compared with the bulk, *ab initio* cluster calculations [28] do suggest a very small amount of vertical relaxation.

The surface of galena is of particular interest because of the problems associated with the processing of ores containing this phase (most processing involves froth flotation and is heavily dependent on surface chemistry) and its potential role as a surface contaminant. Oxidation reactions on the {001} galena surfaces have been extensively studied [28–30]. The intermediate and final products of oxidation are now well known, however, our understanding of the initial oxidation products and mechanisms is less advanced. Becker and Hochella [28] have made some advances in this area using a powerful combination of STM experiments coupled with quantum mechanical cluster calculations of STM images to investigate the reaction of the surface with oxygen. Reactions of galena with oxidising

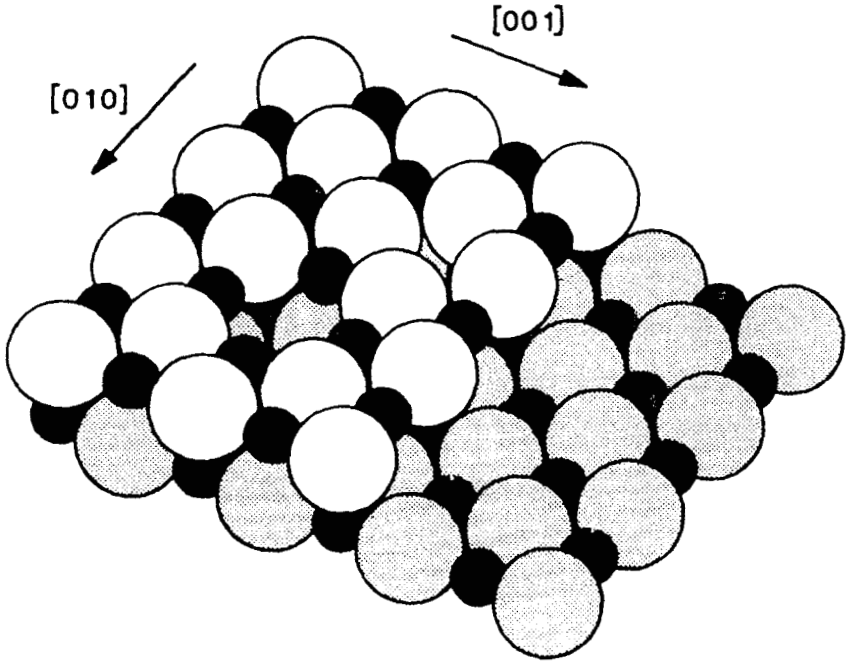

FIGURE 6 The {100} surface of galena, S atoms are large open spheres and Pb atoms small solid spheres. S and Pb vacancies and a step are shown on the upper layer. (After [1]; reproduced with publishers permission).

aqueous fluids appear, not surprisingly, to be dependent on pH and also on any variations in galena stoichiometry. Rates of oxidation are faster for oxygen dissolved in H_2O than for the gas phase, suggesting a role for protons in the oxidation process.

We are currently using a combination of semi-empirical and embedded quantum cluster methods [31] to investigate the dissociation of H_2O molecules on the galena {100} surface. Preliminary results [32] show that H_2O dissociates to form HS and PbOH and that this dissociation takes place only at defect sites and will not occur on the perfect surface. This reaction takes place most readily at a step edge and has a small activation energy of approximately 0.2 eV.

FUTURE WORK

The sulphide minerals are a rich topic for investigation using computer modelling methods, both because of the diversity of their structures and electronic properties, and because of their economic and environmental importance. The availability of a range of computational methods and experimental techniques to tackle problems of sulphide mineral chemistry makes such investigations timely.

We plan to develop both atomistic and quantum mechanical approaches to the investigation of the sulphides. The former, *via* construction of robust potentials, will be used to explore the role played by defects and impurities in influencing bulk and surface properties. The latter, using calculations on clusters, embedded clusters and slabs, will be used to study reactivity and reactions mechanisms at the molecular level.

Acknowledgements

KW thanks NERC and The Royal Society for support through their Fellowship schemes. DJV also thanks NERC for research support. Both authors particularly wish to thank U. Becker, I. H. Hillier, S. C. Parker and G. W. Watson for their help in pursuing various aspects of computational studies of metal sulphides.

References

[1] Tossell, J. A. and Vaughan, D. J. (1992). "Theoretical Geochemistry: Applications of Quantum Mechanics in the Earth and Mineral Sciences", Oxford University Press.

[2] Vaughan, D. J. and Wright, K. V., "Crystal Chemistry of Ore Minerals", In "Modern Approaches to Ore and Environmental Mineralogy" (Cabri, L. J. and Vaughan, D. J. Eds.) *Min. Assoc. of Canada Short Course Notes*, in press.

[3] Bernard, J. E. and Zunger, A. (1987). "Electronic structure of ZnS, ZnSe, ZnTe and their pseudobinary alloys", *Phys. Rev. B*, **36**, 3199.
[4] Engel, G. E. and Needs, R. J. (1990). "Calculations of the structural properties of cubic zinc sulfide", *Phys. Rev. B*, **41**, 7876.
[5] Jaffe, J. E., Pandey, R. and Kunz, A. B. (1991). "Correlated Hartree-Fock electronic structure of ZnO and ZnS", *J. Phys. Chem. Solids*, **52**, 755.
[6] Martins, J. L., Troullier, N. and Wei, S. H. (1991). "Pseudopotential plane-wave calculations for ZnS", *Phys. Rev. B*, **43**, 2213.
[7] Schroer, P., Kruger, P. and Pollmann, J. (1993). "1st principles calculation of the electronic structure of the wurtzite semiconductors ZnO and ZnS", *Phys. Rev. B*, **47**, 6971.
[8] Tossell, J. A. (1977). "Theoretical studies of valence orbital binding energies in solid ZnS, ZnO and ZnF_2", *Inorg. Chem.*, **16**, 2944.
[9] Tossell, J. A. and Vaughan, D. J. (1981). "Relationships between valence orbital binding energies and crystal structures in compounds of copper, silver, gold, zinc, cadmium and mercury", *Inorg. Chem.*, **20**, 3333.
[10] Wright, K. and Jackson, R. A. (1995). "Computer simulation of the structure and defect properties of zinc sulphide", *J. Mater. Chem.*, **5**, 2037.
[11] Catlow, C. R. A. (1986). "Computer simulation studies of transport in solids", *Ann. Rev. Mater. Sci.*, **16**, 517.
[12] Duke, C. B. and Wang, Y. R. (1988). "Surface structure and bonding of the cleavage faces of tetrahedrally coordinated II–IV compounds", *Journal of Vacuum Science and Technology B*, **6**, 1440.
[13] Wright, K., Watson, G. W., Parker, S. C. and Vaughan, D. J., "Simulation of the structure and stability of sphalerite (ZnS) surfaces", *American Mineralogist*, **83**, 141.
[14] Scott, S. D. and Barnes, H. L. (1972). "Sphalerite-wurtzite equilibria and stoichiometry", *Geochim. Cosmochim. Acta*, **36**, 1275
[15] Temmerman, W. M., Durham, P. J. and Vaughan, D. J. (1993). "The electronic structures of the pyrite-type disulphides (MS_2, where M = Mn, Fe, Co, Ni, Cu, Zn) and the bulk properties of pyrite from local density approximation (LDA) band structure calculations", *Phys. Chem. Minerals*, **20**, 248.
[16] Bullett, D. W. (1982). "Electronic structure of 3d pyrite- and marcasite-type sulphides" *J. Phys. C*, **15**, 6163.
[17] Zhao, C. L., Calloway, J. and Hayashibara, M. (1993). "Electronic structure of iron and cobalt pyrites", *Phys. Rev. B*, **48**, 15781.
[18] Zeng, Y. and Holzworth, N. A. W. (1994). "Density functional calculation of the electronic structure and equilibrium geometry of iron pyrite (FeS_2)", *Phys. Rev. B*, **50**, 8214.
[19] Braga, M., Lie, S. K., Taft, C. A. and Lester, W. A. Jr. (1988). "Electronic structure, hyperfine interactions and magnetic properties for octahedral iron sulfides", *Phys. Rev. B*, **38**, 10837.
[20] Wright, K., "New interatomic potentials and calculation of elasticity for FeS_2 Pyrite", in preparation.
[21] Benbattouche, N., Saunders, G. A., Lambson, E. F. and Hönle, W., "The dependences of the elastic stiffness moduli and the Poisson ratio of natural iron pyrites FeS_2 upon pressure and temperature", *J. Phys. D. Appl. Phys.*, **22**, 670.
[22] Hemstreet, L. A. Jr. (1975). "Cluster calculations of the effects of single vacancies on the electronic properties of PbS", *Phys. Rev.*, **B11**, 2260.
[23] Mian, M., Harrison, N. M., Saunders, V. R. and Flavell, W. R. (1996). "An ab initio Hartree-Fock investigation of galena (PbS)", *Chem. Phys. Letts.*, **257**, 627.
[24] Peiris, S. M., Campbell, A. J. and Heinz, D. L. (1994). "Compression of MgS to 54 GPa", *J. Phys. Chem. Solids.*, **55**, 413.
[25] Majewski, J. A. and Vogl, P. (1987). "Simple model for structural properties and crystal stability of *sp*-bonded solids", *Phys. Rev. B*, **35**, 9666.
[26] Hochella, M. F. Jr. (1990). "Atomic Structure, microtopography, composition and reactivity of mineral surfaces", *Miner. Soc. Amer. Rev. Mineral*, **23**, 87.
[27] Eggleston, C. M. and Hochella, M. F. Jr. (1990). "Scanning Tunnelling microscopy of sulfide surfaces", *Geochim. Cosmochim. Acta*, **54**, 1511.

[28] Becker, U. and Hochella, M. F. Jr. (1996). "The calculation of STM images, STS spectra and XPS peak shifts for galena: New tools for understanding mineral surface chemistry", *Geochim. Cosmochim. Acta*, **60**, 2413.
[29] Buckley, A. and Woods, R., "An X-ray photoelectron spectroscopic study of the oxidation of galena", *Appl. Surf. Sci.*, **17**, 401.
[30] Fornasiero, D., Li, F., Ralston, J. and Smart, R. St. C. (1994). "Oxidation of galena surfaces, I. X-ray photoelectron spectroscopic and dissolution kinetics studies", *J. Colloid Interface Sci.*, **55**, 1.
[31] Becker, U., Greatbanks, S. P., Rosso, K. M., Hillier, I. H. and Vaughan, D. J., "An embedding approach for the calculation of STM images: Method development and application to galena (PbS)", *J. Chem. Phys.*, in press.
[32] Wright, K., Hillier, I. H., Vaughan, D. J. and Vincent, M., "The dissolution of H_2O on the surface of galena PbS: a computational study", *Phys. Rev.*, submitted.